Electronic Supplementary Material (ESI) for Inorganic Chemistry Frontiers.

Supporting Information for:

Ternary PdNiMo alloy as bifunctional nanocatalysts for oxygen reduction reaction and hydrogen evolution reaction

Xiao Wu,[†] Xiangnan Liu, Yi He,[†] Lecheng Lei,[†,‡] Shaoyun Hao,*[†] Xingwang Zhang,*[†,‡]

†Key Laboratory of Biomass Chemical Engineering of Ministry of Education, College of Chemical and Biological Engineering Zhejiang University, Hangzhou, Zhejiang Province 310027, China

‡Institute of Zhejiang University-Quzhou, 78 Jiuhua Boulevard North, Quzhou 324000, China

*E-mail: shaoyunhao@zju.edu.cn; xwzhang@zju.edu.cn

Contents

Experimental section

Materials

Materials: $Zn(NO_3)_2 \cdot 6H_2O$, Methanol (CH_3OH), Palladium acetate ($C_4H_6O_4Pd$) and Glucose ($C_6H_{12}O_6$) were all directly obtained from Aladdin Reagent (Shanghai) Co., Ltd. 2-Methylimidazole ($C_4H_6N_2$), $Ni(NO_3)_2 \cdot 6H_2O$, and H_2SO_4 were purchased from Sinopharm Co., Ltd. High purity nitrogen were provided with Hangzhou Metalworking Special Gas Co., Ltd. Carbon paper (CP) was supplied with Shanghai Hesen Electric Co., Ltd. All the reagents applied in this experiment were directly used without any purification. Ultra-pure (18.2 MΩ cm) water was applied to deal with the prepared electrodes and electrolytes.

Characterizations

The surface morphologhies were characterized by SU-80 microscope (Hitachi) scanning electron microscopy (SEM) with a field emission source. Micrographs of transmission electron microscopy (TEM), High-resolution TEM (HR-TEM) imaging and energy-dispersive X-ray (EDX) spectroscopy, were obtained by Tecnai G2 F20 S-TWIN (FEI, America), equipped with an X-ray energy dispersive spectrometer with a field emission source at 200keV. XRD analysis was performed on the crystal structures of the samples by Bruker D8 Venture X-ray diffractometer with Cu-Kα (λ =1.54178 Å) as radiation source. X-ray photoelectron spectroscopy (XPS) was obtained using VG ESCALAB with a monochrome Al anode (Al Kα = 1486.6 eV) to examine the surface nanocatalysts. The multielement content of as-synthesized samples was determined by inductively coupled plasma (ICP) using the Aglient 7300DV ICP-OES. Raman scattering spectra was performed on nanocatalysts by ZTJD6-13471HK (Cryo Industries of America, Inc.) with the 514.5 nm

line of Ar^+ for excitation.

Electrochemical Measurements

Electrochemical characterizations including cyclic voltammetry (CV), Linear sweep voltammetry (LSV) and chronopotentiometry were carried out on a CHI 760D electrochemical instrument using a three-electrode electrochemical system. The platinum column electrode and Hg/Hg_2SO_4 full of saturated K_2SO_4 solution were, respectively, employed as counter and reference electrodes. Linear sweep voltammetry (LSV) was applied to characterize the performances of these prepared electrodes in an electrolytic cell containing 0.1 M $HClO_4$ with bubbling O_2 or N_2 for 30 min at the scan rate of 10 mV s^{-1} with the rotation rates varied from 400 to 2250 rpm. The CV measurements were carried out in O_2-saturated 0.1 M $HClO_4$ solution at the potential scan rate of 100 mV s^{-1}.

Chronoamperometric (current vs. time (*i-t*) curves) measurements were conducted in an O_2-saturated 0.1 M $HClO_4$ solution at 0.5 V (vs. RHE) for 35,000s. The number of electrons transferred in ORR can be calculated from the slope of Koutecky-Levich plot, which was constructed in accordance with the Koutecky-Levich equation. The electron transfer number during ORR was calculated by Koutecky-Levich equation [1]:

$$1/J = 1/J_K + 1/J_L = nFkC_0 + 1/B\omega^{1/2} \quad (3)$$

$$B = nFC_0D^{2/3}v^{-1/6} \quad (4)$$

Where J is the measured current density, J_K and J_L are the kinetic and diffusion-limiting current densities, ω is the angular velocity, n is transferred electron number, F is Faraday constant (96485 C mol^{-1}), C_0 is the bulk concentration of O_2 (1.2×10^{-6} mol cm^{-3}), D_0 is the diffusion coefficient of O_2 in 0.1 M $HClO_4$ (1.93×10^{-5} cm^2 s^{-1}), and v is the kinetic viscosity of the electrolyte (0.01 cm^2 s^{-1}).

The electrochemically active surface area (ECSA) was estimated by measuring the charge

associated with H_{upd} desorption, and the ECSA was calculated based on the following equation:

$$ECSA = S_H/mvq_H \quad (5)$$

Where S_H, m, v, and q_H are the peak area of H_{upd} desorption, the weight of the Pd loading, scan speed, and the charge (210 μC cm^{-2}) required for monolayer adsorption of hydrogen on a Pd surface, respectively.

Specific activity (SA) and mass activity (MA) are used to calculate the ORR catalytic activity of Pd alloy catalyst based on the catalyst kinetic current at 0.9 V vs. RHE.

$$SA = J_K/(ECSA \times m_{Pd}) \quad (6)$$

$$MA = J_K/(m_{Pd}) \quad (7)$$

Where J_K and m_{Pd} are the kinetic current density and m_{Pd} is the Pd loading on the tested RDE, respectively.

In an HER test, catalyst (1.2 mg) and carbon black (1.2 mg) were dispersed in a mixture containing 2.2 mL ethanol and 0.6 mL Milli-Q water. Subsequently, 0.2 mL 5% Nafion solution was added into the mixture as a binder and the mixture was ultrasonicated for 1 h, then the obtained ink (1 mL) was consistently dispensed onto the carbon paper (1 × 1 cm) at room temperature. The Pd loadings for Pd/NC, Pd_2Ni/NC, Pd_3Ni/NC, Pd_4Ni/NC, $Mo_{0.1}Pd_3Ni$/NC, $Mo_{0.2}Pd_3Ni$/NC, $Mo_{0.3}Pd_3Ni$/NC and Pt/C were 19.16 μg_{Pd} cm^{-2}, 18.96 μg_{Pd} cm^{-2}, 19.24. μg_{Pd} cm^{-2}, 20.04 μg_{Pd} cm^{-2}, 18.64 μg_{Pd} cm^{-2}, 20.11 μg_{Pd} cm^{-2}, 21.08 μg_{Pd} cm^{-2}, and 40 μg_{Pt} cm^{-2}, respectively. LSV was collected in 0.5 M H_2SO_4 N_2-saturated solution at the scan rate of 10 mV s^{-1}. Moreover, all the applied potentials were calibrated by a reversible hydrogen electrode (RHE). The electrochemical impedance was obtained using electrochemical impedance spectroscopy (EIS) over the frequency domain of 0.01 Hz to 100,000 Hz. The AC potential amplitude applied in EIS measurements was 5 mV. R_s was obtained by the equivalent circuit fitting EIS data using ZSimpWin software. All the HER

electrochemical tests were in the three-electrode system with a graphite rod and mercurous sulfate electrode, employed as counter and reference electrodes. Furthermore, the potentials were *iR*-corrected to compensate the effect of uncompensated solution resistance R_s using the following equation:

$$E_{iR\text{-corrected}} = E_{applied} - iR_s \quad (8)$$

Where i is current on the electrode.

The double-layer capacitance (C_{dl}) is calculated from CV measurements by the equation:

$$C_{dl} = (J_a - J_c) / (2 \times v) = (|J_a| + |J_c|) / (2 \times v) = \Delta J/(2 \times v) \quad (9)$$

Where J_a and J_c are the anodic and cathodic current density recorded at the middle of the selected potential range and v is the sweep rate.

The roughness factor (R_f) was calculated by using the equation:

$$R_f = C_{dl}/C_s \quad (10)$$

The ECSA of the catalysts were estimated from C_{dl} by the equation:

$$ECSA = A_0 \times C_{dl}/C_s \quad (11)$$

Where the C_s, assumed to 35 μF cm^{-2} based on typical reported value, is the specific capacitance of the sample or the capacitance of an atomically smooth planar surface of the material per unit area under identical electrolyte conditions. A_0 is the geometric surface area of the working electrode.

Calculation of Faradaic efficiency

To calculate Faradaic efficiency of $Mo_{0.2}Pd_3Ni$/NC in 0.5 M H_2SO_4 solution toward HER, Test was carried out in a three-electrode configuration and detected by a gas chromatography (GC, 9790II, Hangzhou Gatai Scientific Instruments). Firstly, electrolyte and cell were degassed with Ar under stirring for 30 min. Secondly, a constant current of 5 mA was applied for a period. Using a gas tight syringe to draw gas sample from the head space and the sample

was analyzed by a GC calibrated for H_2. Each gas sample was tested at least three times and the result of each injection was calculated to obtained the average value.

The Faradaic efficiency (*FE*) is calculated based on the following equation:

$$FE = (2 \times V_{H2} \times F) / (V_m \times I \times t) \times 100\% \quad (12)$$

V_{H2} is the evolved volume of H_2, F is the Faraday constant (96485.33289 C/mol), V_m is the molar volume of the gas, I is the current, and t is the time for electrolysis.

Theoretical calculations

Density function theory (DFT) calculation details: To preliminarily explore the activity of each catalyst, Vienna Ab Initio Package (VASP) [2, 3] was used to perform all the spin-polarized density functional theory (DFT) calculations within the generalized gradient approximation (GGA) using the Perdew-Burke-Ernzerhof (PBE) [4] formulation. We have chosen the projected augmented wave (PAW) potentials [5, 6] to describe the ionic cores and take valence electrons into account using a plane wave basis set with a kinetic energy cutoff of 500eV. Partial occupancies of the Kohn-Sham orbitals were allowed using the Gaussian smearing method and a width of 0.01 eV. The electronic energy was considered self-consistent when the energy change was smaller than 10^{-5} eV. The maximum Hellmann-Feynman force for each ionic optimization step is 0.01eV/Å, as well as the optimization of equilibrium lattice constants. Spin-polarization was considered in all calculations [7].

Two configurations of catalysts are established, named Mo-doped, $NiPd_3$ and Pd. There are four active site candidates for Mo-doped samples, two possible active sites $NiPd_3$ for sample and one catalytic center for Pd sample. A 3×3×1 Gamma k-point grid for Brillouin zone sampling was used in energy calculation. This slab was separated by a 20 Å vacuum layer in

the Z direction between the slab and its periodic images. In order to fully consider the activity of each catalyst, the possible catalytic sites in catalysts are selected to discuss their adsorption behavior.

The free energy (ΔG) of ORR on those catalysts was defined as

$$\Delta G = E_{DFT} + E_{ZPE} - T \times S \quad (13)$$

where E_{DFT}, E_{ZPE}, T and S are the calculation total energy of *O, *OH, and *OOH intermediate on catalysts surface, the zero-point energy, temperature, and entropy.

The overpotential (η^{ORR}) of ORR was defined as:

$$\eta^{ORR} = \max\{\Delta G1, \Delta G2, \Delta G3, \Delta G4\}/e + 1.23 \quad (14)$$

where the ΔG1, ΔG2, ΔG3, ΔG4 are the free energy for four elementary reactions of ORR.

Table S1. The yield of each prepared catalyst

Name	yield
Pd/NC	84.12%
Pd_2Ni/NC	84.53%
Pd_3Ni/NC	85.66%
Pd_4Ni/NC	84.27%
$Mo_{0.1}Pd_3Ni$/NC	85.83%
$Mo_{0.2}Pd_3Ni$/NC	82.58%
$Mo_{0.3}Pd_3Ni$/NC	83.47%

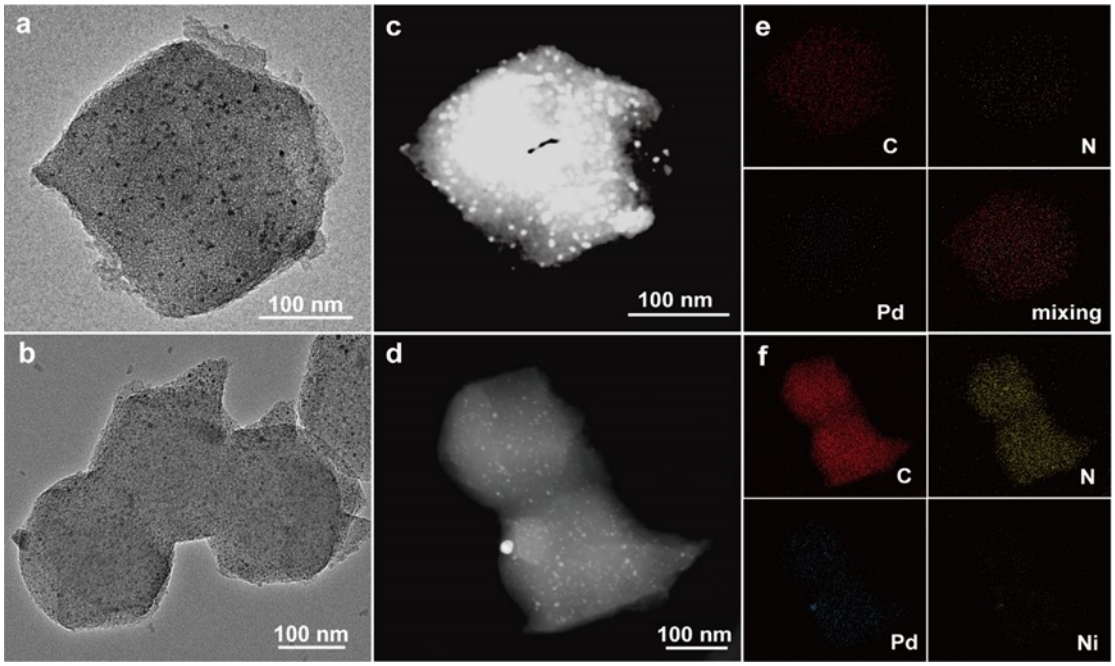

Figure S1. (a-b) TEM images, (c-d) STEM images, (e-f) corresponding elemental distribution mapping of Pd/NC, and Pd_3Ni/NC.

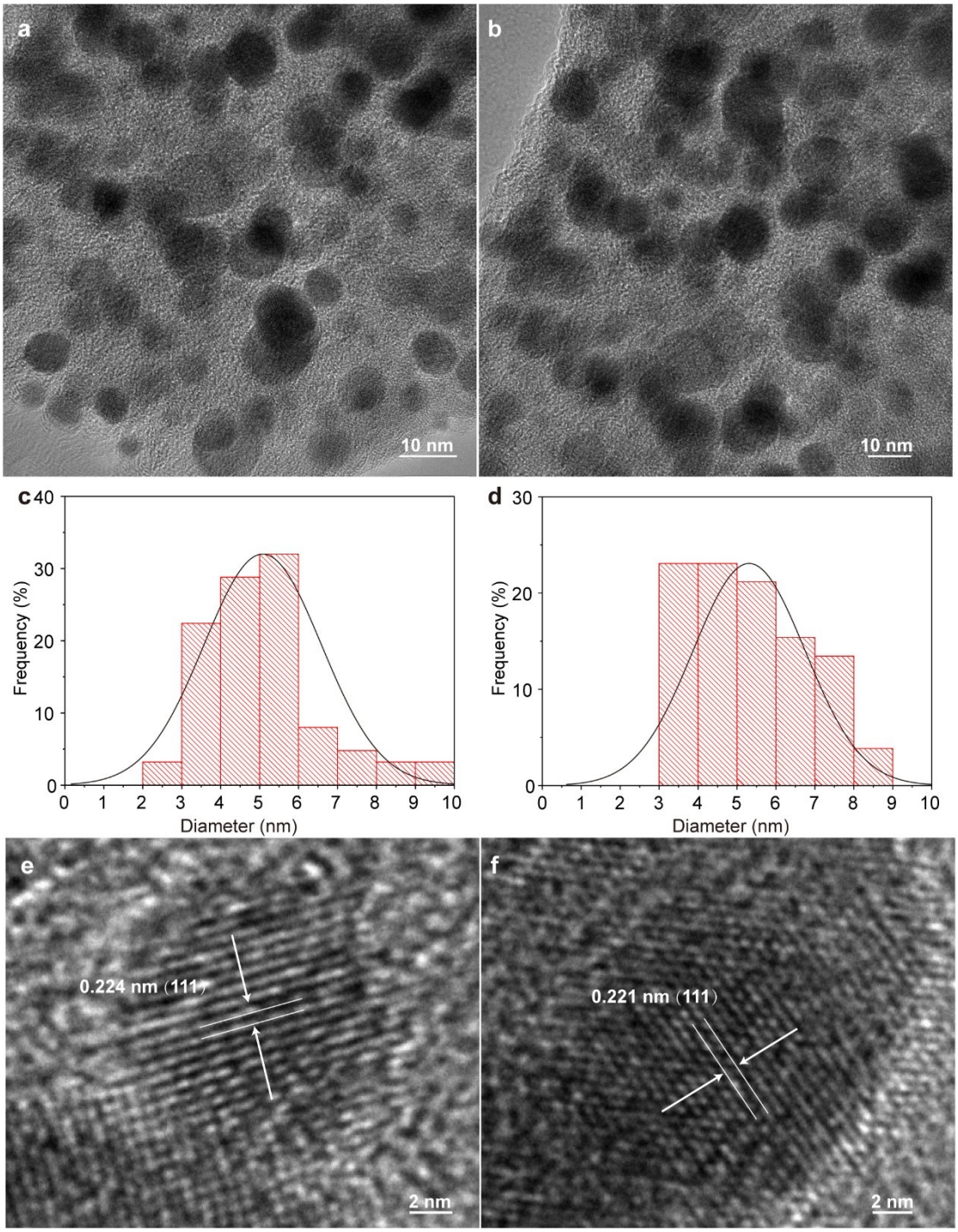

135

136 **Figure S2**. (a-b) TEM images, (c-d) corresponding size distribution histograms, (e-f) HR-

137 TEM images of Pd/NC, and Pd_3Ni/NC.

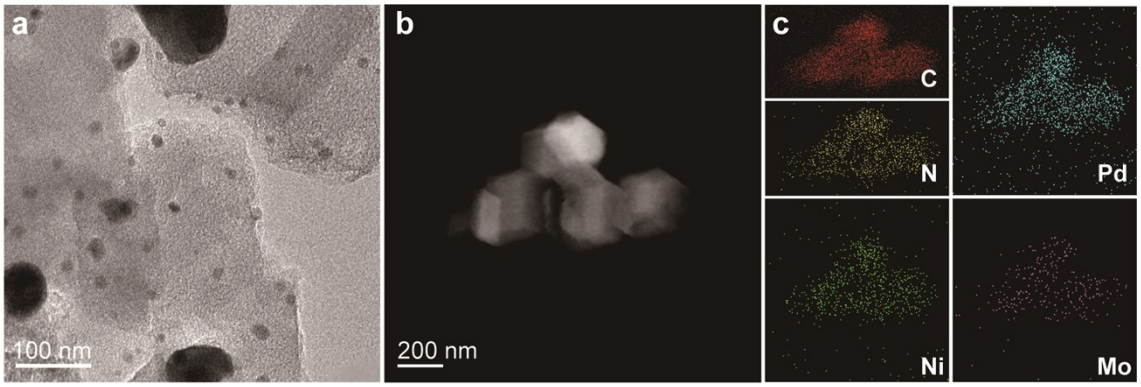

Figure S3 (a) TEM image, (b) STEM image, (c) corresponding elemental distribution mapping of $Mo_{0.2}Pd_3Ni$/NC after the reaction.

142

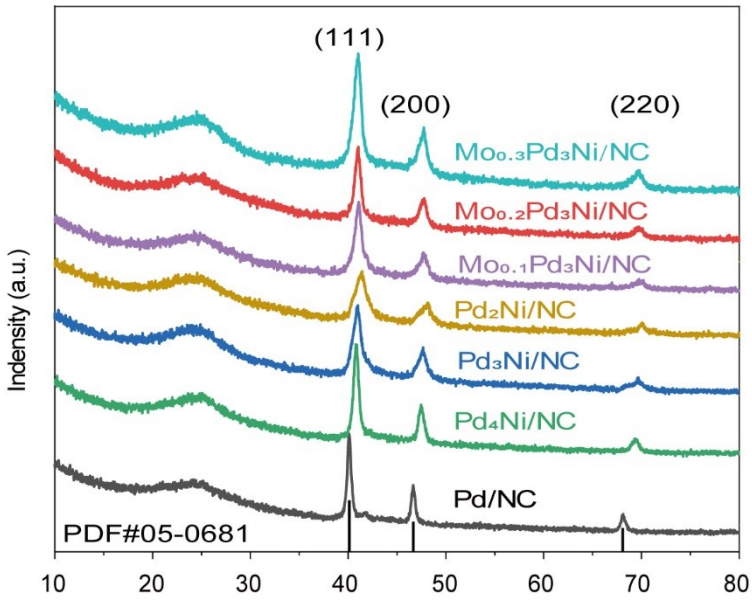

143 **Figure S4**. The XRD patterns of all the prepared Pd-based nanocatalysts.

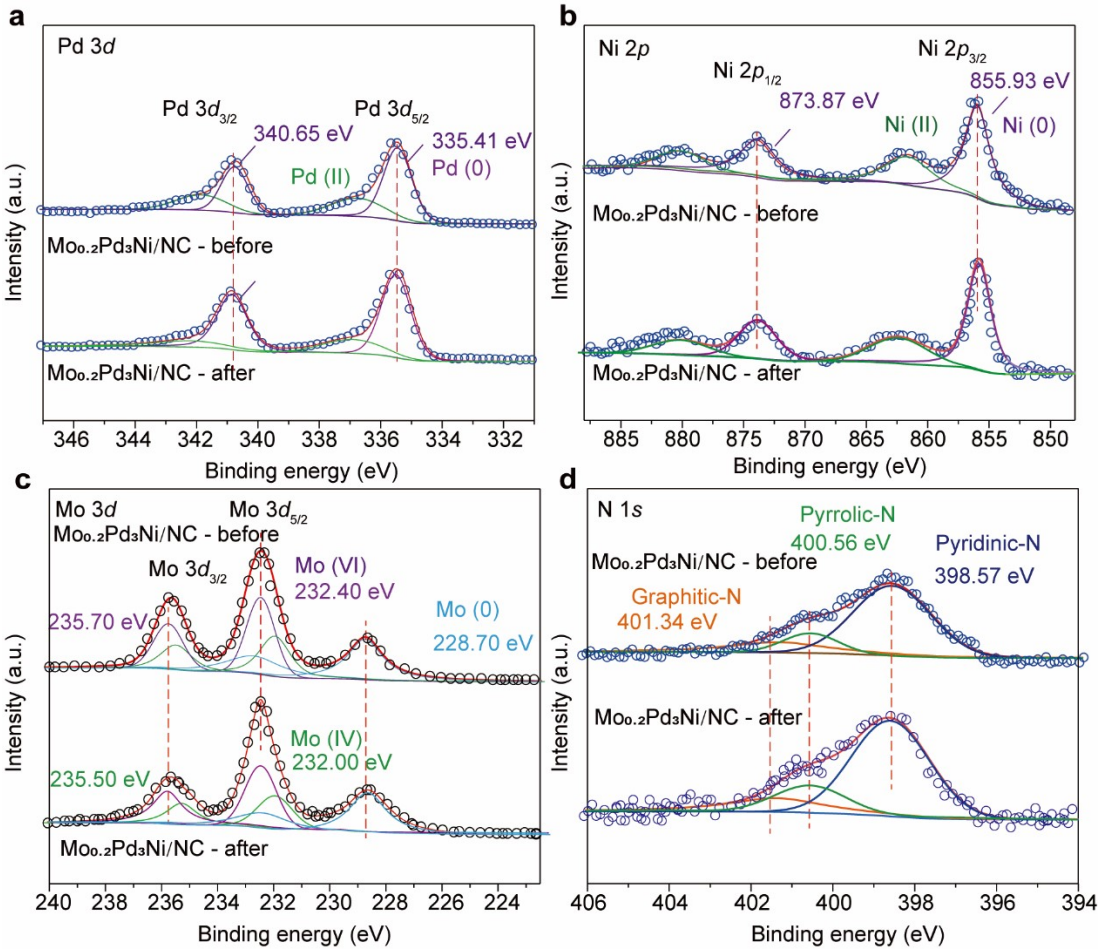

Figure S5. (a) Pd 3*d*, (b) Ni 2*p*, (c) Mo 3*d*, (d) N 1*s* XPS spectra of $Mo_{0.2}Pd_3Ni$/NC before and after the reaction, respectively.

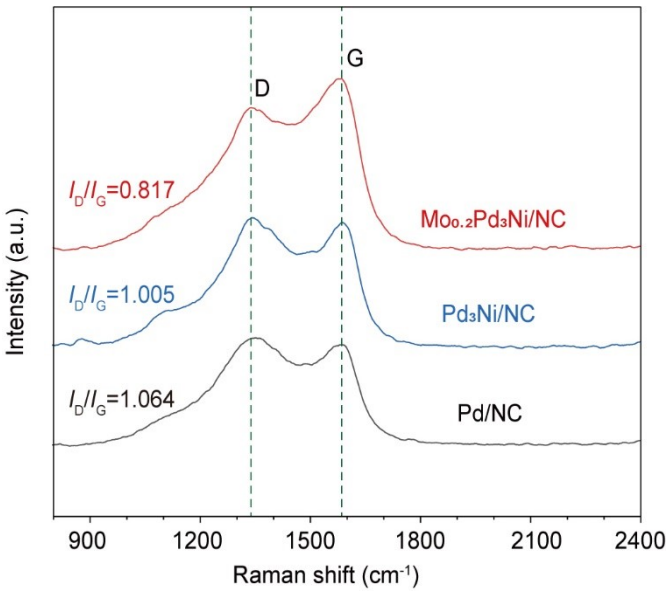

150

151 **Figure S6**. Raman spectra for Pd/NC, Pd_3Ni/NC, and $Mo_{0.2}Pd_3Ni$/NC nanocatalysts.

153 **Table S2** ICP-OES analysis of the prepared Pd/NC, Pd_3Ni/NC and $Mo_{0.2}Pd_3Ni$/NC

154 nanocatalysts

Catalysts	Element	Sample amount	Element Content	wt.%
Pd/NC	Pd	15.0 mg	100051.2 mg/kg	10.01
Pd_3Ni/NC	Pd	15.0 mg	100259.5 mg/kg	10.03
	Ni	15.0 mg	18576.3 mg/kg	1.86
$Mo_{0.2}Pd_3Ni$/NC	Pd	15.0 mg	99835.5 mg/kg	9.98
	Ni	15.0 mg	18435.2 mg/kg	1.84
	Mo	15.0 mg	6067.9 mg/kg	0.61

Table S3 Binding energy and chemical state of Pd 3*d* spectra for Pd/NC, Pd_3Ni/NC, and $Mo_{0.2}Pd_3Ni$/NC nanocatalysts

Catalysts	Binding energy Pd $3d_{5/2}$ (eV)	Binding energy Pd $3d_{3/2}$ (eV)	Chemical state
Pd/NC	335.57	340.84	Pd (0)
	337.00	342.12	Pd (II)
Pd_3Ni/NC	335.48	340.80	Pd (0)
	336.93	342.05	Pd (II)
$Mo_{0.2}Pd_3Ni$/NC	335.41	340.65	Pd (0)
	336.72	341.81	Pd (II)

Table S4 Binding energy and chemical state of Ni 2*p* spectra for Pd_3Ni/NC, and $Mo_{0.2}Pd_3Ni/NC$

Catalysts	Binding energy Ni $2p_{3/2}$ (eV)	Binding energy Ni $2p_{1/2}$ (eV)	Chemical state
Pd_3Ni/NC	855.40	873.04	Ni (0)
	863.22	881.24	Ni (II)
$Mo_{0.2}Pd_3Ni/NC$	855.93	873.87	Ni (0)
	862.69	880.71	Ni (II)

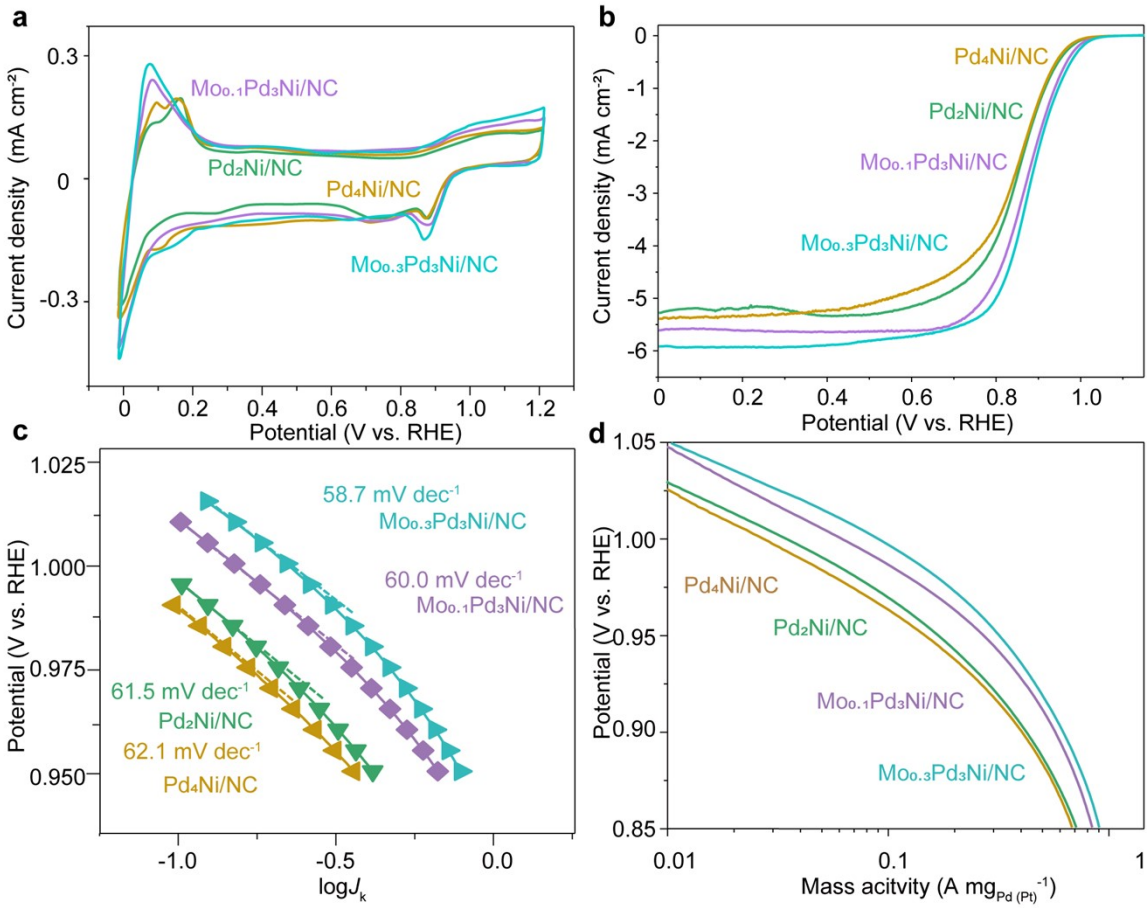

Figure S7. (a) CV curves, (b) LSV curves, (c) Tafel plots, and (d) Mass activity of Pd_2Ni/NC, Pd_4Ni/NC, $Mo_{0.1}Pd_3Ni/NC$, and $Mo_{0.3}Pd_3Ni/NC$ nanocatalysts in 0.1 M KOH solution.

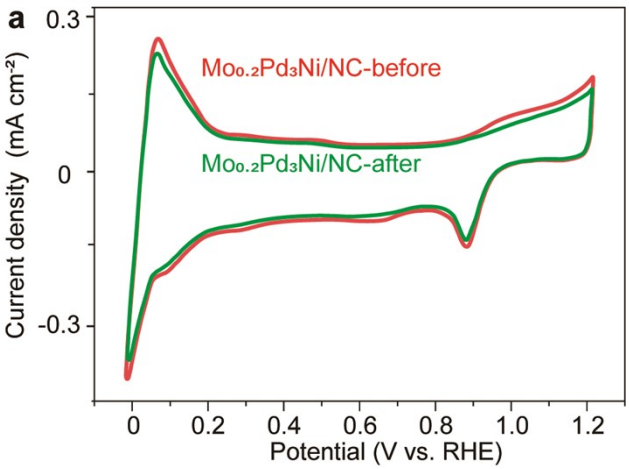

169

170 **Figure S8.** CV curves of $Mo_{0.2}Pd_3Ni$/NC before and after the reaction, respectively.

172 **Table S5** Onset potential, diffusion limiting current density, and half-wave potential of all the

173 prepared nanocatalysts and Pt/C

Catalysts	E_{onset} (V vs. RHE)	Current density (mA cm^{-2})	$E_{1/2}$ (V vs. RHE)
Pd/NC	0.92	4.92	0.82
Pd_4Ni/NC	0.94	5.38	0.84
Pd_3Ni/NC	0.96	5.53	0.87
Pd_2Ni/NC	0.95	5.23	0.85
$Mo_{0.1}Pd_3Ni$/NC	0.97	5.59	0.87
$Mo_{0.2}Pd_3Ni$/NC	0.99	5.89	0.90
$Mo_{0.3}Pd_3Ni$/NC	0.97	5.92	0.88
Pt/C	1.01	5.82	0.90

175 **Table S6** Comparison of ORR performances in alkaline media with previous works

Catalysts	E_{onset} (V vs. RHE)	$E_{1/2}$ (V vs. RHE)	MA (A mg_{Pd}^{-1}) (0.9 V)	Reference
$Mo_{0.2}Pd_3Ni$/NC	0.99	0.90	0.78	This work
PdNi nanocorals	0.949	0.851	0.006 A	*Part. Part. Syst. Char.*, **2018**, 35: 1700366.
Dealloyed PdNi/C	/	0.87	0.37 (0.85 V)	*ACS Catal.*, **2020**, 10: 5891.
$Pd_{50}Cu_{50}$ film	/	0.886	0.13	*J. Am. Chem. Soc.*, **2020**, 142: 3980.
Ordered PdCuCo	/	0.872	0.13	*Angew. Chem., Int. Ed.*, **2016**, 55: 9030.
Dendritic defect-rich $Pd_{59}Cu_{30}Co_{11}$	/	0.91	0.38	*Nat. Commun.*, **2018**, 9: 3702.
PdCoNi/NCNTs	0.970	0.907	0.252	*Chem. Eng.J.*, **2021**, 411: 128527.
PdMo bimetallene/C	/	0.95	16.37	*Nature*, **2019**, 574: 81.

176

178 **Table S7** Mass activities of all the prepared nanocatalysts and Pt/C at 0.9 V and 0.85 V

Catalysts	Mass activity (0.9 V) (A mg_{Pd}^{-1})	Mass activity (0.85 V) (A mg_{Pd}^{-1})
Pd/NC	0.29	0.55
Pd_4Ni/NC	0.40	0.68
Pd_3Ni/NC	0.52	0.82
Pd_2Ni/NC	0.42	0.71
$Mo_{0.1}Pd_3Ni$/NC	0.57	0.84
$Mo_{0.2}Pd_3Ni$/NC	0.78	1.01
$Mo_{0.3}Pd_3Ni$/NC	0.62	0.90
Pt/C	0.38 (A mg_{Pt}^{-1})	0.49 (A mg_{Pt}^{-1})

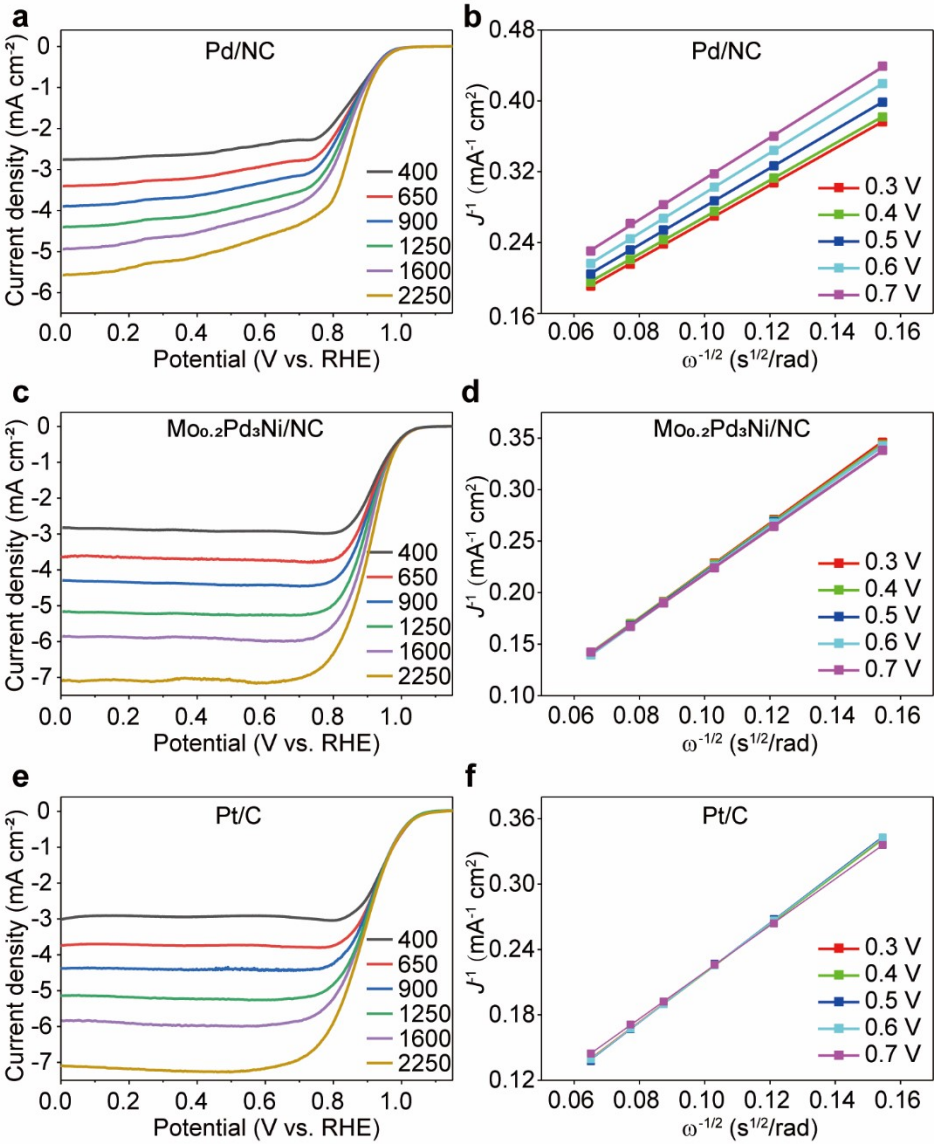

180

181 **Figure S9**. LSV curves of (a) Pd/NC, (c) $Mo_{0.2}Pd_3Ni$/NC, (e) Pt/C in O_2-saturated 0.1 M

182 KOH solution at a different rotation rate from 400-2250 rpm. Koutecky-Levich (K-L) plots of

183 (b) Pd/NC, (d) $Mo_{0.2}Pd_3Ni$/NC, (f) Pt/C.

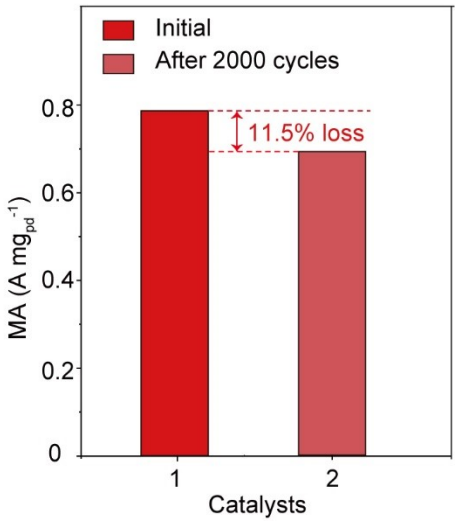

185

186 **Figure S10**. Initial and after 2000 cycles mass activities values of $Mo_{0.2}Pd_3Ni$/NC.

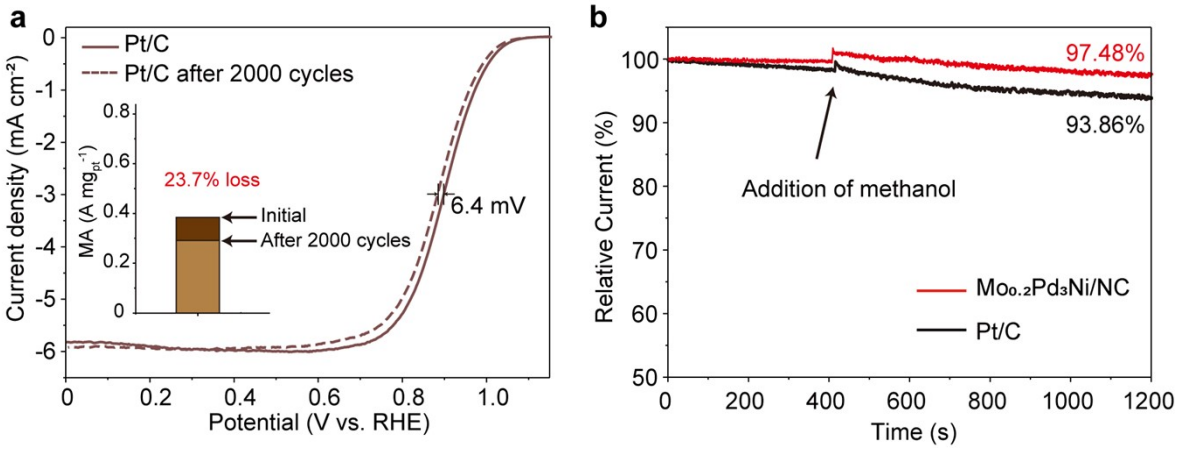

188

189 **Figure S11**. (a) ADT measurement, (b) methanol tolerance test of $Mo_{0.2}Pd_3Ni$/NC and Pt/C

190 in 0.1 M KOH solution.

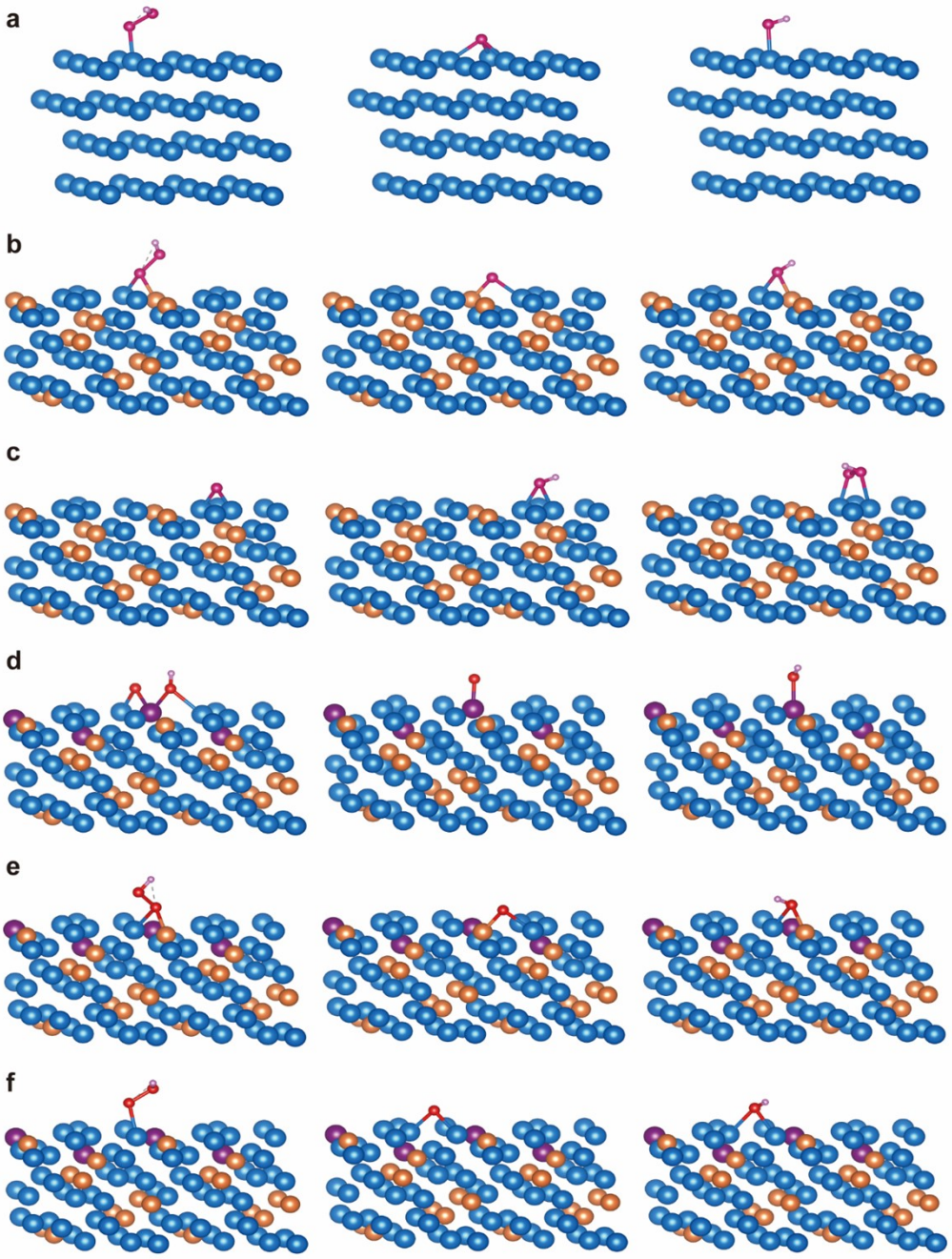

Figure S12. (a) Configurations of adsorbed intermediates on Pd (b) Configurations of adsorbed intermediates on Pd_3Ni active site 1 (c) Configurations of adsorbed intermediates on Pd_3Ni active site 2 (d) Configurations of adsorbed intermediates on $Mo_{0.2}Pd_3Ni$ active site 1 (e) Configurations of adsorbed intermediates on $Mo_{0.2}Pd_3Ni$ active site 3 (f) Configurations of adsorbed intermediates on $Mo_{0.2}Pd_3Ni$ active site 4.

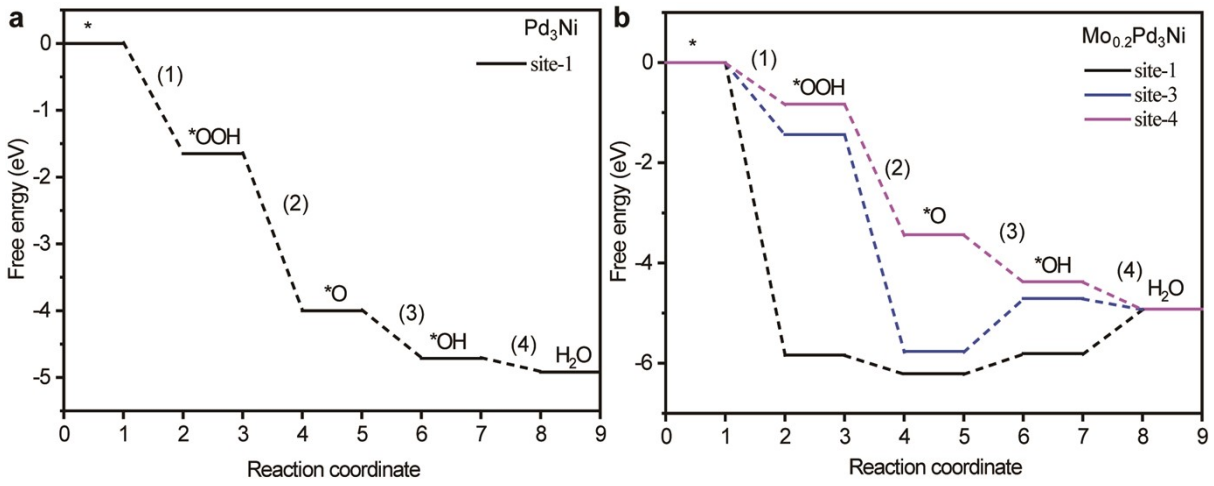

Figure S13. (a) Free energy diagrams of Pd_3Ni active site-1. (b) Free energy diagrams of $Mo_{0.2}Pd_3Ni$ active site-1, site 3 and site-4.

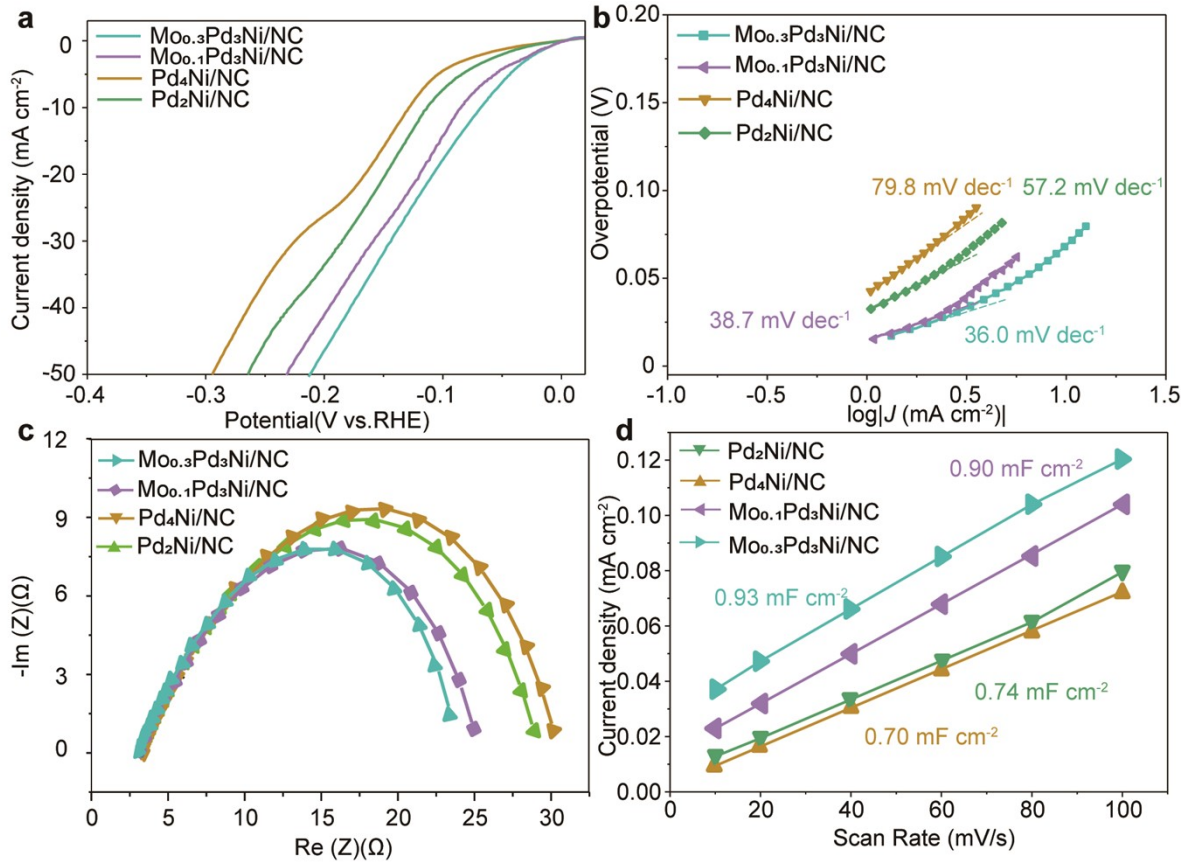

203

204 **Figure S14**. (a) LSV curves (b) The Tafel plots (c) EIS Nyquist plots (d) C_{dl} of Pd_2Ni/NC,

205 Pd_4Ni/NC, $Mo_{0.1}Pd_3Ni/NC$, and $Mo_{0.3}Pd_3Ni/NC$ for HER in 0.5 M H_2SO_4.

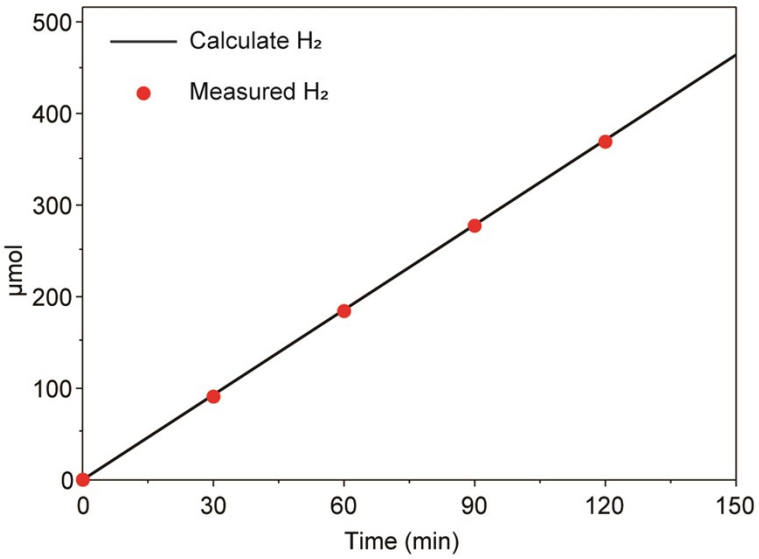

207

208 **Figure S15**. Hydrogen accumulation of $Mo_{0.2}Pd_3Ni$/NC in 0.5 M H_2SO_4.

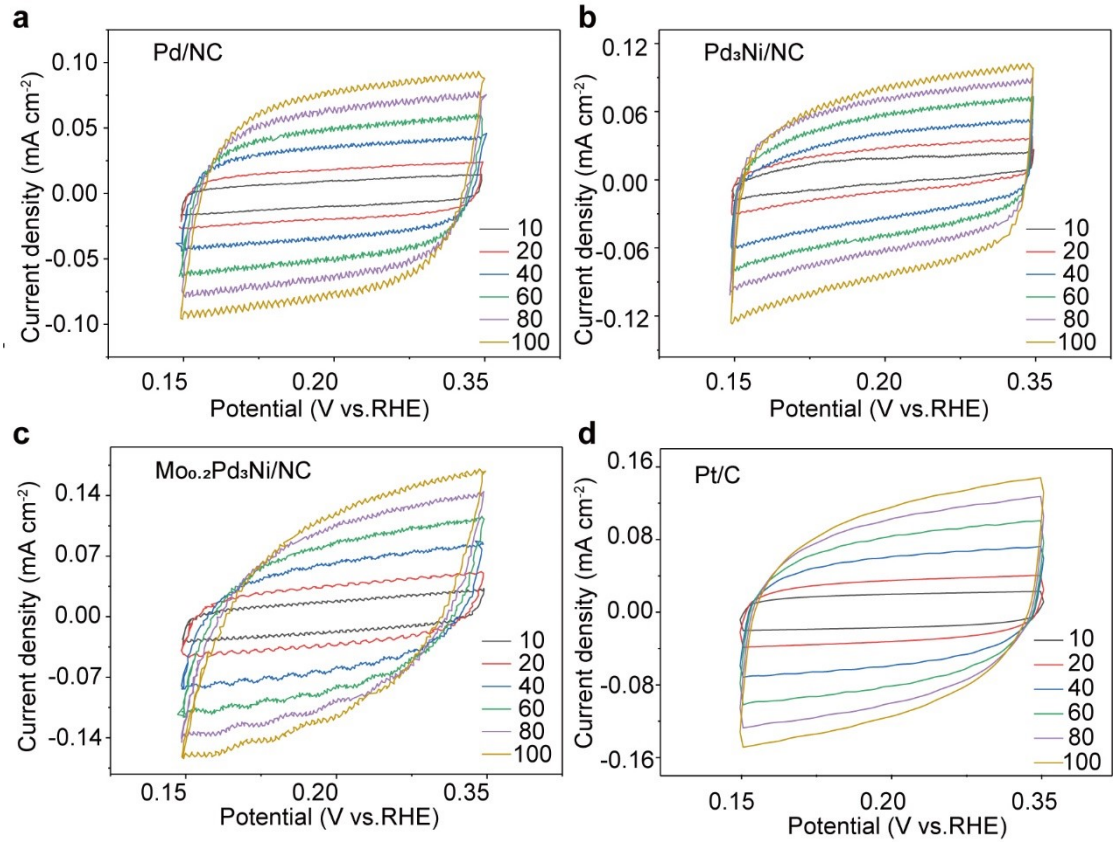

Figure S16. CV curves of the representative prepared catalysts and Pt/C in 0.5 M H_2SO_4.

Table S8 Comparison of HER performance in acid media from previous reports

Catalysts	Overpotentials at 10 mA cm^{-2}	Tafel slop ($mV\ dec^{-1}$)	Media	Reference
$Mo_{0.2}Pd_3Ni$@NC	53	35.8	0.5 M H_2SO_4	This work
Cu-Pd-S	52	39	0.5 M H_2SO_4	*Advanced Fiber Materials*. **2021**, 3: 117-127.
Pd_2Te NWs/rGO	48	63	0.5 M H_2SO_4	*Nanoscale,* **2015**, 7, 18441-18845.
$PdCu_{1.3}$ alloy nanoparticles	50	34	0.5 M H_2SO_4	*ACS Catal,* **2016**, 6, 1929.
Pd nanoparticle−graphitic carbon nitride	53	35	0.5 M H_2SO_4	*ACS App. Mater. Interfaces,* **2016**, 8, 13378.
PdCu@Pd NCs	65	35	0.5 M H_2SO_4	*ACS Appl. Mater. Interfaces,* **2017**, 499, 128.
Pd-c-NiCo-PBA-C	147	67	0.5 M H_2SO_4	*Adv. Funct. Mater,* **2021**, 31: 2008989.

Reference:

1 S. Treimer, A. Tang, D.C. Johnson, *Electroanalysis*, 2002, **14**, 165-171.

2 L. Zhu, C. Ma, Z. Wang, X. Gong, L. Cao, J. Yang, *Applied Surface Science*, 2022, **576**, 151840.

3 G. Kresse, J. Furthmüller, Efficient iterative schemes for ab initio total-energy calculations using a plane-wave basis set, *Physical Review B*, 1996, **54**, 11169-11186.

4 J.P. Perdew, K. Burke, M. Ernzerhof, *Physical Review Letters*, 1996, 77, 3865-3868.

5 G. Kresse, D. Joubert, *Physical Review B*, 1999, **59**, 1758-1775.

6 P.E. Blöchl, *Physical Review B*, 1994, **50**, 17953-17979.

7 L. Gong, D. Zhang, C.-Y. Lin, Y. Zhu, Y. Shen, J. Zhang, X. Han, L. Zhang, Z. Xia, *Advanced Energy Materials*, 2019, **9**, 1902625.